# Adsorption and photocatalytic oxidation of ibuprofen using nanocomposites of TiO2 nanofibers combined with BN nanosheets: Degradation products and mechanisms

Lu Lin, Wenbin Jiang, Mikhael Bechelany, Maryline Nasr, Jacqueline Jarvis, Tanner Schaub, Rishi Sapkota, Philippe Miele, Huiyao Wang, Pei Xu

1    **Adsorption and photocatalytic oxidation of ibuprofen using nanocomposites of TiO₂**

2    **nanofibers combined with BN nanosheets: degradation products and mechanisms**

3

4    Lu Lin[1], Wenbin Jiang[1], Mikhael Bechelany[2], Maryline Nasr[2], Jacqueline Jarvis[3], Tanner

5    Schaub[3], Rishi R. Sapkota[3], Philippe Miele[2], Huiyao Wang[4*], Pei Xu[1*]

6

7    [1]Department of Civil Engineering, New Mexico State University, 3035 S Espina Street, Las

8    Cruces, NM 88003, USA

9    [2]Institut Européen des Membranes, IEM, UMR-5635, Université de Montpellier, ENSCM,

10    CNRS, Place Eugène Bataillon, F-34095 Montpellier Cedex 5, France

11    [3]Chemical Analysis and Instrumentation Laboratory, College of Agricultural, Consumer and

12    Environmental Sciences, New Mexico State University, Las Cruces, NM 88003, USA

13    [4]Core University Research Resources Laboratory, New Mexico State University, Las Cruces,

14    NM 88003, USA

15

16    *Corresponding author: Dr. Huiyao Wang, Email: huiyao@nmsu.edu

17    *Corresponding author: Dr. Pei Xu, Email: pxu@nmsu.edu

18

19

20  **Abstract**

21   This study investigated the adsorption and photocatalytic activity of $TiO_2$-boron nitride (BN)

22  nanocomposites for the removal of contaminants of emerging concern in water using ibuprofen

23  as a model compound. $TiO_2$ nanofibers wrapped by BN nanosheets were synthesized by

24  electrospinning method. Characterization of the nanocomposite photocatalysts indicated the BN

25  nanosheets improved the light absorbance and reduced the recombination of the photoexcited

26  charge carriers ($e^-$ and $h^+$). The photocatalytic oxidation products and mechanisms of ibuprofen

27  by the $TiO_2$-BN catalysts were elucidated using a multiple analysis approach by high

28  performance liquid chromatography, ultraviolet absorbance, dissolved organic carbon,

29  fluorescence excitation-emission matrices, and electrospray ionization–liquid chromatography–

30  tandem mass spectrometry. The experimental results revealed that the photocatalytic oxidation

31  by the $TiO_2$-BN nanocomposites is a multi-step process and the interactions between ibuprofen

32  molecules and the $TiO_2$-BN nanocomposites govern the adsorption process. The increasing BN

33  nanosheet content in the $TiO_2$ nanofibers facilitated the breakdown of ibuprofen degradation

34  intermediates (hydroxyibuprofen, carboxyibuprofen, and oxypropyl ibuprofen). Kinetic

35  modeling indicated both adsorption and photocatalytic oxidation of ibuprofen by the $TiO_2$-BN

36  nanocomposites followed the first-order kinetic model. The photocatalytic oxidation rate

37  increased with the increasing BN content in the nanocomposite catalysts, which was attributed to

38  the light absorption capacity and the separation efficiency of the photoexcited electron ($e^-$)-hole

39  ($h^+$) pairs. Multiple photocatalytic cycles were conducted to investigate the reusability and

40  regeneration of the nanofibers for degradation of ibuprofen.

41

## 1. Introduction

Contaminants of emerging concerns such as pharmaceuticals and personal care products (PPCPs) have been widely detected in water bodies around the world (Vieno et al., 2007). Many PPCPs are of serious concerns even in trace amounts due to their toxicity to aquatic life and potential risks to public health (Vieno et al., 2007; Christen et al., 2010). Conventional water and wastewater treatment processes including coagulation, sedimentation, media filtration, and biological processes are not effective to remove these recalcitrant organic contaminants (Vieno et al., 2007; Xiang et al., 2016). Adsorption by activated carbon is an efficient technique to remove hydrophobic PPCPs through hydrophobic interactions, however the adsorption capacity gradually decreases as the carbon is saturated with the adsorbed chemicals. In addition, it is ineffective to adsorb hydrophilic compounds such as atenolol, acetaminophen, and naproxen (Vieno et al., 2007; Huerta-Fontela et al., 2011; Wang et al., 2015). Oxidation using chlorine, chlorine dioxide, and ozone is typically effective to degrade PPCPs with electron-donating functional groups (e.g., phenolic-and amine-containing compounds) (Lee and von Gunten, 2010). Ultraviolet (UV) irradiation can degrade many PPCPs but treatment cost is inhibitive because of high energy demand (Rosenfeldt and Linden, 2004).

To degrade the persistent organic contaminants, advanced oxidation processes (AOPs) are typically needed (De la Cruz et al., 2012). AOPs generate hydroxyl radicals ($\cdot$OH) which react non-selectively with most organic compounds (Andreozzi et al., 1999). Commonly used AOPs for PPCPs removal from wastewater include $UV/H_2O_2$, $UV/O_3$, (photo)-Fenton, and heterogeneous photocatalysis (De Witte et al., 2009; Homem and Santos, 2011; Prieto-Rodriguez et al., 2012; Carbonaro et al., 2013; Van Doorslaer et al., 2015; Thagard et al., 2016). Complete mineralization is usually not the goal of AOPs because it is energy intensive and not cost-

67    effective (Doll and Frimmel, 2004). Partial degradation of recalcitrant PPCPs is more

68     economically attractive to deactivate their biological activity or increase their biodegradability

69    (Van Doorslaer et al., 2015). But more concerns are raised regarding the intermediate

70    degradation products and their environmental toxicities.

71    Heterogeneous photocatalytic oxidation using metal oxides (e.g., $TiO_2$) has attracted

72    considerable attention particularly due to its potentially lower cost than other AOPs (Jing et al.,

73    2006; Dalrymple et al., 2007; Rubio et al., 2013; Lin et al., 2015; Arlos et al., 2016; Lin et al.,

74    2016; Lin et al., 2017b; Lin et al., 2017f; Li and Hu, 2018). More than 90 organic and 25

75    inorganic compounds catalogued on the US Environmental Protection Agency's (USEPA)

76    priority list of contaminants have been investigated using heterogeneous photocatalysis (Blake,

77    2001), such as acetone, aniline, atrazine, benzene, methyl tertiary butyl ether (MTBE),

78    trichloroethane. The process has also been successfully applied for the treatment of organic and

79    inorganic compounds at low concentrations in aqueous solutions (Wold, 1993; Nakajima et al.,

80    2005; Westerhoff et al., 2005; Le-Clech et al., 2006).

81    During heterogeneous photocatalysis, organic molecules adsorb onto a metal oxide catalyst

82    surface and react with the photoexcited charge carriers ($e^-$ and $h^+$) or free radicals (e.g., $\cdot OH$)

83    (Ollis et al., 1984; Kormann et al., 1991). The photocatalytic reaction depends on the species of

84    organic molecules adsorbed onto the photocatalyst surface and in aqueous phase, which results in

85    different kinetics of photodegradation. As a critical step in heterogeneous photocatalysis, very

86    few studies investigated the kinetics of organics adsorption on a photocatalyst (Bauer et al., 2001;

87    Vautier et al., 2001; Hu et al., 2003; Yu et al., 2005; Lee et al., 2011; Zhang et al., 2013; Rioja et

88    al., 2014; Lv et al., 2016).

89    Titanium dioxide ($TiO_2$) is the most commonly used photocatalyst due to its relatively low cost,

90    high stability, and low toxicity (Fujishima et al., 2000; Kumar and Devi, 2011a; Nakata and

91    Fujishima, 2012). Substantial efforts have been devoted to improve the photocatalytic

92    degradation efficiency of $TiO_2$ through combination with metal ions, non-metal ions, and some

93    2D nanomaterials (Liqiang et al., 2006; Rubio et al., 2013; Lin et al., 2015; Arlos et al., 2016;

94    Lin et al., 2016; Lin et al., 2017b; Lin et al., 2017f; Li and Hu, 2018; Yi et al., 2018; Merenda et

95    al., 2019). These dopants, such as Ag (Harifi and Montazer, 2014), Fe (Asiltürk et al., 2009; Lin

96    et al., 2016), P (Zhang et al., 2012), $SiO_2$ (Tawkaew and Supothina, 2008), and graphene (oxide)

97    (Lin et al., 2017c; Lin et al., 2017d; Yi et al., 2018), have been proven to be effective to improve

98    the photocatalytic activity. A recent study reported that the boron nitride (BN) nanosheets exhibit

99    unique properties due to the high surface area and the reactive edge structure (Biscarat et al.,

100   2015). Previous study demonstrated that the introduction of BN nanosheets enhanced the

101   separation of electron–hole pairs of $TiO_2$ and dramatically improved photocatalytic activity of

102   methyl orange under ultraviolet (UV) irradiation (Nasr et al., 2017b).

103   This study aims to investigate the mechanisms and kinetics of adsorption and photocatalytic

104   oxidation of PPCPs using novel photocatalytic composite $TiO_2$ nanofibers with boron nitride

105   (BN) nanosheets. Combining $TiO_2$ with BN nanosheets by electrospinning method is anticipated

106   to enhance the separation of $e^-$-$h^+$ pairs of $TiO_2$ thus to improve the photocatalytic activity.

107   Ibuprofen, a nonsteroidal anti-inflammatory drug that has been found extensively in wastewater

108   effluents, was used as the target recalcitrant PPCP. The adsorption and degradation of ibuprofen

109   by photolysis and photocatalysis was characterized by a series of analytical methods.

110   Degradation intermediates of ibuprofen were analyzed by a positive ion electrospray ionization–

111   liquid    chromatography–tandem    mass    spectrometry    [(+)  ESI  LC-MS/MS].    Multiple

112　photocatalytic cycles were conducted to evaluate the recyclability and regeneration of the $TiO_2$-

113　BN nanocomposites for the degradation of ibuprofen.

114

115　**2. Materials and methods**

116　2.1　　Materials and characterization

117　A series of BN nanosheets incorporated $TiO_2$ nanofibers (0, 3%, 5%, 7%, and 10%, weight

118　percentage of BN to the mass of Ti, referred as $TiO_2$, TB1, TB2, TB3, and TB4, respectively)

119　were synthesized using electrospinning technique as described by Nasr et al. (2017b). UV-Vis

120　absorbance of the nanofibers was measured by a spectrophotometer (DR6000; Hach Company,

121　CO). X-ray diffraction (XRD) measurements were conducted using a PANAlytical Xpert-PRO

122　diffractometer equipped with an X'celerator detector using Ni-filtered Cu-radiation. The specific

123　surface area of the nanocomposites was determined from the nitrogen adsorption–desorption

124　isotherms measured at liquid nitrogen temperature using a Micromeritics ASAP 2010

125　(outgassing conditions: 200 °C and 12 h). The structure and morphology of the nanocomposite

126　catalysts was characterized by an H-7650 transmission electron microscope (TEM; Hitachi High-

127　Technologies Corp., Pleasanton, CA). The elemental mapping images were taken with a Zeiss

128　EVO HD15 microscope coupled with an Oxford X-MaxN EDX detector.

129

130　2.2　　Adsorption and photodegradation experiments

131　Ibuprofen (Analytical grade; Acros Organics Co, NJ) was used as a model compound

132　representative of PPCPs to evaluate the adsorption and photocatalytic activity of the synthesized

133　nanocomposites. The pH of the tested ibuprofen solution was neutral throughout the experiments.

134    Batch experiments were conducted in 100 mL beakers containing a suspension of 10 mg

135    nanofibers and 50 mL ibuprofen solution (5 mg $L^{-1}$) under dark (adsorption), UV light

136    irradiation with nanofibers (photocatalysis) or without nanofibers (photolysis) conditions. The

137    irradiance of UV lamp (160W PUV-10, Zoo Med Laboratories, San Luis Obispo, CA) included

138    both UV (365 nm, minor peaks at 290, 315, 335 nm) and visible light (405, 435, and 545 nm)

139    wavelength spectrum. The solution mixtures were magnetically stirred for 2 to 3 hours, and 1 mL

140    water samples were taken at 0, 10, 20, 30, 60, 90, 120, and 180 min. The suspensions were then

141    filtered through 0.45 μm cellulose acetate membrane to separate nanofibers for analysis. All

142    adsorption, photolysis, and photocatalytic degradation experiments under each condition were

143    conducted at least two times to ensure the reproducibility of the results.

144    Repeated ibuprofen degradation experiments were conducted for 16 cycles to evaluate the

145    recyclability of the $TiO_2$-BN nanocomposites under 3-hour UV light irradiation. Because the

146    filtration and the centrifugation were not effective to collect all the nanocomposites from the

147    solution, the suspensions were dried at 80 °C overnight after each degradation experiment to

148    evaporate water from the ibuprofen and nanofibers mixture solution. Fresh ibuprofen solution

149    was then added to the dried nanocomposites to repeat the photocatalytic experiment.

150

151    2.3    Analytical methods

152    The adsorption and degradation of ibuprofen were characterized by a high-performance liquid

153    chromatography (HPLC; PerkinElmer Series 200, CT, USA), UV absorbance at 254 nm ($UV_{254}$),

154    and dissolved organic carbon (DOC) quantified through a carbon analyzer (Shimadzu TOC-L,

155    Kyoto, Japan). Specific UV absorbance (SUVA) was quantified by dividing the $UV_{254}$ by the

156    corresponding DOC concentration of ibuprofen samples, which indicates the change of aromatic

157     structure of ibuprofen molecules. Fluorescence excitation-emission matrix (FEEM) spectroscopy

158     was used to obtain information on characteristics of ibuprofen and potential degradation

159     products in water samples (Aqualog-UV-800-C; Horiba Instruments Inc., NJ).

160     The intermediate products of the ibuprofen degradation were further investigated using a (+) ESI

161     LC-MS/MS method with an Ultimate 3000 nano-flow LC system coupled to an Orbitrap Fusion

162     mass spectrometer equipped with an Adivon NanoMate nano-electrospray ionization source.

163     The LC solvent system consisted of water with 0.1% formic acid (A) and acetonitrile with 0.1%

164     formic acid (B).  The gradient was 2% B at 0 min to 95% B at 60 min with a 10 min 95% B flush

165     and 20 min equilibration between samples.  Data-dependent Orbitrap MS2 mass spectra (HCD

166     Energy = 27%, RP = 30000) were collected with a 3-sec cycle time between parent scans (m/z

167     100-1000, RP = 120000).  Easy-IC lock mass calibration was used for parent scans.  Background

168     ion signals were excluded from tandem mass spectrometry.  Accurate mass measurement for

169     parent ions (e.g. <1 part per million, ppm) was used to constrain tandem mass spectral library

170     matching and impart high confidence to the matched results. Tandem mass spectra were searched

171     against the 2017 NIST tandem MS library and only matches within 1 ppm precursor mass

172     tolerance, 0.5 m/z product ion mass tolerance, a reverse match factor > 700, and C# < 13 were

173     considered robust matches.

174

175     2.4     Adsorption and photocatalytic kinetic models

176     Adsorption kinetics are usually governed by film diffusion and intra-particle diffusion (Lu Lin,

177     2014; Xuesong Xu, 2015; Lin et al., 2017g). However, the adsorption kinetics in this study are

178     complex due to the desorption of ibuprofen molecules from nanofibers with weak adsorption

179     bonding energy. Thus, the adsorption capacity and the rate to reach the equilibrium

180     concentration were investigated using a commonly used kinetic model: the pseudo first-order

181     kinetic model.

182     Typically, the performance of $TiO_2$ photocatalysis is usually characterized by Langmuir–

183     Hinshelwood kinetic model (Turchi and Ollis, 1990; Ollis et al., 1991; Coleman et al., 2000;

184     Tanaka et al., 2000; Houas et al., 2001; Li et al., 2006; Kumar and Devi, 2011b). It describes a

185     pseudo-first-order kinetics when the initial concentration of ibuprofen is low (millimolar) (Houas

186     et al., 2001; Konstantinou and Albanis, 2004) (Eq. 1):

187
$$ln\left(\frac{C_0}{C}\right) = k_{app}t \qquad (1)$$

188     where $C_0$ and $C$ are the initial and real-time ibuprofen concentrations (mg L$^{-1}$) at time $t$ (min),

189     $k_{app}$ is the apparent pseudo-first-order rate constant (min$^{-1}$).

190

191     **3. Results and discussion**

192     3.1      Characterization of the synthesized catalysts

193     As shown in Figure 1, the peaks in XRD spectra were referred to primary anatase $TiO_2$ phase in

194     the synthesized catalysts with presence of trace amount of rutile $TiO_2$ phase. Energy dispersive

195     X-ray spectra (EDX) indicated the amounts of elements B and N increased with increasing BN

196     dose in the $TiO_2$-BN nanocomposites (Nasr et al., 2017a). However, the XRD patterns of $TiO_2$-

197     BN nanocomposites were similar to the pure $TiO_2$, suggesting the doping of BN had marginal

198     impact on $TiO_2$ crystallization during electrospinning process.

199   The elemental mapping images revealed that Ti, O, B and N elements were evenly distributed

200   over the entire area of the synthesized materials (Nasr et al., 2017a). The morphological and

201   structural features of the synthesized materials were examined by TEM as shown in Figure S1.

202   The $TiO_2$-BN nanocomposites with different BN doses all displayed in a similar fiber form. The

203   crystallite size of the nanofibers can be determined by Scherrer equation (Lin et al., 2017e). The

204   crystallite sizes of the $TiO_2$-BN nanocomposites increased slightly with the increasing BN dose

205   (24.3-28.7 nm), while the particle size of pure $TiO_2$ was the smallest of 16.4 nm (Table 1). The

206   increasing trend of grain sizes was also observed by scanning electron microscopy (SEM)

207   images in previous study (Nasr et al., 2017a). This can be attributed to the increase of the

208   solution viscosity induced by inclusion of BN in the electrospinning solution (Nalbandian et al.,

209   2015). This increase revealed the successful incorporation of BN in $TiO_2$ nanofibers. Besides,

210   previous XPS analysis of $TiO_2$-BN nanocomposite suggested the formation of chemical B-O-Ti

211   bond between a titanium atom of $TiO_2$ and a boron atom at the edge of BN in $TiO_2$-BN

212   nanocomposite (Liu et al., 2017).
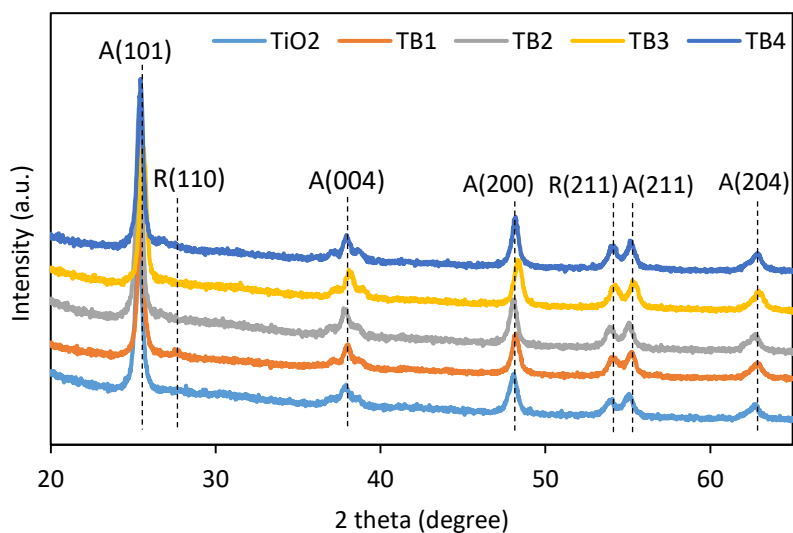
213



214                     Figure 1. XRD patterns of synthesized catalysts. A: anatase; R: rutile.

215

216    The specific surface area of the synthesized nanocomposites increased from 19.7 $m^2$ $g^{-1}$ to 49.6

217    $m^2$ $g^{-1}$ with the increasing dose of BN nanosheets in the composites (Table 1). In general,

218    materials with a large surface area can accelerate adsorption process due to more active

219    adsorption sites available (Lin et al., 2017a). In addition, the UV-Vis absorption spectra of $TiO_2$,

220    TB1, TB2, TB3, and TB4 measured in previous study (Nasr et al., 2017a) demonstrated that the

221    incorporation of BN nanosheets improved the light absorbance of the $TiO_2$-BN nanocomposites

222    in the range of 350-550 nm, which corresponds to the irradiance peak of the UV lamp used in the

223    present work. As such, a higher photocatalytic performance could be expected by combining

224    $TiO_2$ nanofibers with BN nanosheets. The increased light absorption efficiency resulted in an

225    enhanced photocatalytic activity, which was further evidenced by the degradation of ibuprofen

226    using $TiO_2$-BN nanocomposites in Section 3.3.

227

228                    Table 1. Characterization of the synthesized nanocomposites

| Photocatalysts | $TiO_2$ | TB1 | TB2 | TB3 | TB4 |
|---|---|---|---|---|---|
| Specific surface area ($m^2$ $g^{-1}$) | 19.7 | 31.8 | 34.4 | 48.3 | 49.6 |
| Crystalline size (nm) | 16.4 | 24.3 | 25.2 | 26.3 | 28.7 |

229

230    3.2    Adsorption kinetics of the synthesized catalysts

231    The adsorption kinetics for ibuprofen onto different photocatalysts are shown in Figure 2.

232    Ibuprofen molecules adsorbed onto photocatalysts from the aqueous solution increased quickly

over time, and the equilibrium was achieved within 90 min for all photocatalysts. Adsorption onto synthesized nanocomposites showed the same inverted "L" shape, indicating a similar kinetic adsorption process. The adsorption capacity of these catalysts varied in the range of 40-65% after 3-hour adsorption. Ibuprofen had better affinity and higher adsorption with pure $TiO_2$ than with $TiO_2$-BN nanocomposites.

The model parameters and the coefficients of determination ($R^2$) of the pseudo first-order kinetic equation were calculated based on the experimental data, and the results are summarized in Table 2 (modeling curves are presented in Supporting Information Figure S2). The kinetic model fitted well to the experimental data with the coefficients of determination ($R^2$) higher than 0.8. The amount of adsorbed ibuprofen at equilibrium ($q_e$) was approximately 14 mg $g^{-1}$ for all nanocomposites, except for TB4 (10.3 mg $g^{-1}$). Pure $TiO_2$ achieved the highest adsorption kinetic rate constant ($k_1 = 0.106$ min$^{-1}$), which was 10 times larger than that of TB1. The adsorption kinetic rate constants followed the order of $TiO_2$ > TB2 > TB3 > TB4 > TB1, which was similar to the tendency observed in Figure 2.
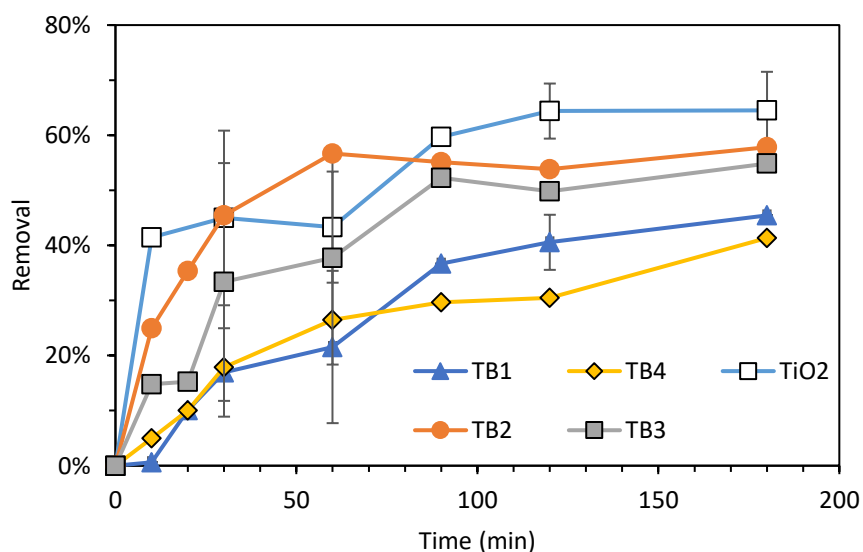
248  Figure 2. Adsorption kinetics of ibuprofen onto different photocatalysts. Error bars represent the

249  standard deviation of duplicate experiments.

250

251  Generally, wrapping BN nanosheet onto $TiO_2$ nanofibers is expected to raise the ibuprofen

252  adsorption onto the photocatalyst due to the larger specific surface area (Table 1). However, the

253  interactions between ibuprofen and the nanocomposite catalysts also govern the adsorption

254  process. Lee *et al.* proposed that the adsorption mechanism between $TiO_2$ and organics involved

255  the electrostatic (H-bonding) and the covalent (bidentate-bridging mode) bonding (Lee et al.,

256  2011). The surface complex was formed via H-bonding with $TiOH/Ti-OH_2$ (Ti-O) and COO-

257  (COOH) groups (Lee et al., 2011). Besides, ibuprofen is negatively charged with the acid-base

258  logarithmic ionization constant $pK_a$ of 4.85 at neutral pH (Lin et al., 2017a). $TiO_2$ nanofibers are

259  nearly neutral at pH 7 with the point of zero charge $pH_{pzc}$ of 6.4, while the BN nanosheets are

260  hydrophilic and negatively charged (Lin et al., 2010). As such, the introduction of BN increased

261  the electrical repulsion between ibuprofen and the catalysts, resulting in lower adsorption. In

262  addition, smaller particle size of pure $TiO_2$ (Table 1) may contribute to higher ibuprofen

263  adsorption because smaller dimension often facilitates adsorption (Yean et al., 2005).

264

265  Table 2. Kinetic parameters for adsorption and photocatalytic activity of the pure $TiO_2$ and $TiO_2$-

266  BN nanocomposites

| Catalyst | Adsorption | | | Photocatalysis | |
|---|---|---|---|---|---|
| | $k_1$ (min$^{-1}$) | $q_e$ (mg g$^{-1}$) | $R^2$ | $k_{app}$ (min$^{-1}$) | $R^2$ |

| | | | | | |
|---|---|---|---|---|---|
| TiO$_2$ | 0.106 | 14.13 | 0.836 | 0.047 | 0.994 |
| TB1 | 0.010 | 13.95 | 0.974 | 0.028 | 0.985 |
| TB2 | 0.052 | 14.1 | 0.996 | 0.033 | 0.979 |
| TB3 | 0.024 | 13.77 | 0.964 | 0.041 | 0.975 |
| TB4 | 0.015 | 10.28 | 0.974 | 0.054 | 0.952 |

267

268 3.3 Photocatalytic kinetics of the synthesized catalysts

269 The photodegradation of ibuprofen under UV irradiation is shown in Figure 3. The degradation

270 efficiency of direct photolysis (no catalyst) was measured under the same conditions for

271 photocatalysis (with catalyst). After 120 min of UV light exposure, there was 27% degradation

272 of ibuprofen without catalyst. It suggests that ibuprofen molecules can absorb UV light in the

273 region of lamp emission. On the other hand, photodegradation of ibuprofen remarkably improved

274 due to the enhancing effect of the nanocomposites under the UV irradiation. After 2 h of UV

275 light exposure, ibuprofen was almost completely degraded in the presence of photocatalysts.
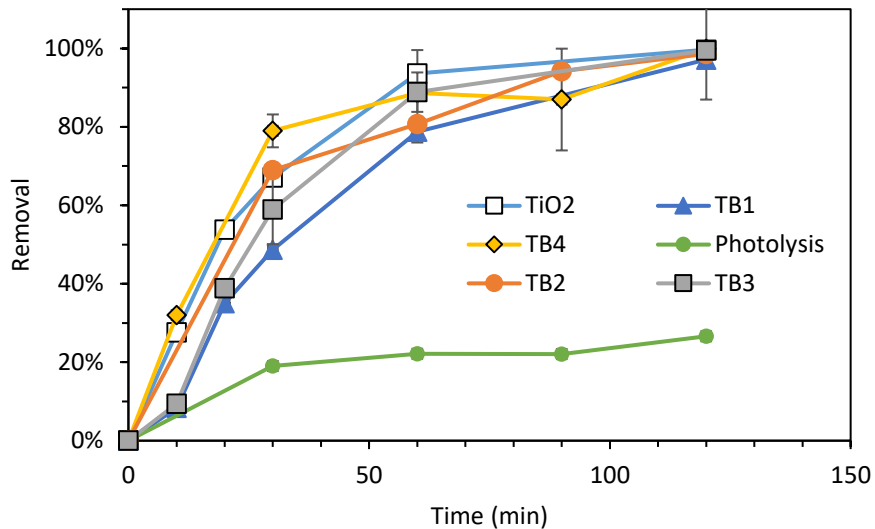
276

Figure 3. Photocatalytic kinetics of ibuprofen onto different photocatalysts under UV light
irradiation. Error bars represent the standard deviation of duplicate experiments.

Langmuir-Hinshelwood kinetic model (Eq. 1) was applied to the photocatalytic data. A plot of $\ln(C_0/C)$ *versus* time t for ibuprofen degradation is presented in Figure 4, and the kinetic parameters are listed in Table 2. The Langmuir–Hinshelwood kinetic model fitted well the experimental data and the coefficients of determination ($R^2$) obtained were greater than 0.9. The photocatalytic activity presented a similar trend as BN content, except for pure $TiO_2$. As shown in Table 2, the apparent photocatalysis rate of TB4 (0.054 $min^{-1}$) was higher than pure $TiO_2$ (0.047 $min^{-1}$), while $TiO_2$ had higher adsorption kinetics rate ($TiO_2$ 0.059 vs. TB4 0.039 $min^{-1}$). Hence, TB4 exhibits excellent photocatalytic activity for ibuprofen removal rather than adsorption. The photocatalytic degradation rates of $TiO_2$ and TB2 were lower than adsorption rates, inferring that their adsorption rate is faster than the photocatalytic oxidation rate, so oxidation is the control step for the photocatalytic reaction. On the contrary, adsorption is the

16

291    control step for TB1, TB3, and TB4 photocatalysis. This was further demonstrated by the

292    multiple photocatalysis cycles discussed in Section 3.6.
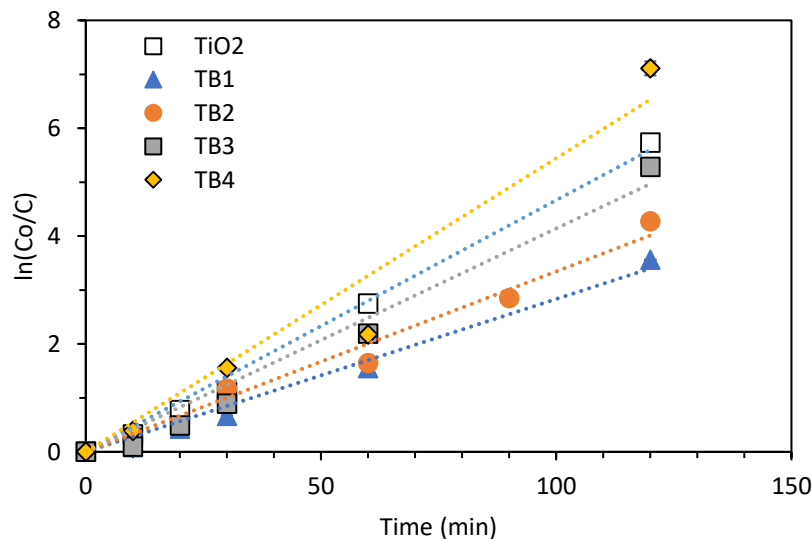


293

294    Figure 4. Langmuir-Hinshelwood kinetic modeling curves of ibuprofen degradation by the

295    synthesized nanocomposites

296

297    Adsorption has both positive and negative impacts on photocatalysis. On the one hand, more

298    adsorbed ibuprofen molecules on the catalyst surface improve the transfer of photogenerated

299    radicals, which explained why the photocatalytic degradation rate of $TiO_2$ was slightly higher

300    than TB1 and TB2. On the other hand, the photocatalytic activity is mainly affected by light

301    absorption capacity and separation efficiency of $e^-$-$h^+$ pairs. The adsorbed ibuprofen may hinder

302    the photocatalysis degradation by screening the light access to the catalysis, so photocatalytic

303    degradation rate of $TiO_2$ was relatively low even with the highest adsorption rate. The

304    photocatalytic degradation rate of $TiO_2$-BN nanocomposite increased with the increasinng BN

305    content probably due to enhanced light absorption intensity (Section 3.1). Meanwhile, due to

306  electrostatic interactions, the negatively charged BN nanosheets surface can lead to the transfer

307  of $h^+$ from the $TiO_2$ particles to the BN nanosheets. As such, the recombination of $e^-$ and $h^+$ is

308  inhibited with increasing BN dose, which was confirmed by previous photoluminescence study

309  (Nasr et al., 2017a).

310

311  3.4    Ibuprofen degradation intermediates and proposed pathway

312  Aiming at identifying the degradation intermediates, (+) ESI LC-MS/MS was performed to

313  detect the constituents in the ibuprofen solutions after photocatalytic treatment. Figure 5 showed

314  extracted-ion chromatographic peak areas for ibuprofen degradation intermediates (including

315  hydroxyibuprofen, carboxyibuprofen, and oxypropyl ibuprofen) after 2-hour UV irradiation. The

316  proposed photocatalytic degradation pathway of ibuprofen is present in Figure 6. All compounds

317  shown were confirmed by high resolution mass spectrometry, where elemental composition of

318  the parent ions was determined from accurate m/z measurement and tandem mass spectrometry

319  indicates molecular structure. For simplicity, only one isomer among several possible is shown at

320  each step. Some intermediates are proposed to be formed by successive free radical

321  hydroxylation followed by oxidation to yield the carbonyl compounds (aldehyde and ketone).

322  The primary carbon oxidation to carboxylic acid is a facile process and that product is confirmed

323  by our mass spectrometry results. The most reactive site of the ibuprofen molecule in the

324  presence of free radical (˙OH) is the benzylic carbon, which gives monohydroxylated ibuprofen

325  (confirmed by mass spectrometry). Once the benzylic hydroxyl ibuprofen is formed, it undergoes

326  further oxidation to give the beta-keto acid. Beta keto acids are susceptible for decarboxylation

327  and results the formation of oxypropyl ibuprofen. A similar oxidation decarboxylation route for

328  the degradation of ibuprofen has been reported in the literature (Skoumal et al., 2009).

329  As presented in Figure 3, the sample under direct photolysis (no catalyst) displayed the lowest

330  removal of ibuprofen (27% in 2-hour UV irradiation) and relatively low amounts of degradation

331  intermediates (Figure 5). It suggested only a small fraction of ibuprofen was oxidized and the

332  degradation process was limited to the initial degradation levels. Degradation in the existence of

333  photocatalysts is more complete since both ibuprofen and its degradation products can be

334  adsorbed onto the catalysts. From Figure 3, ibuprofen was almost completely degraded in the

335  presence of photocatalysts after 2-hour UV light exposure, but the amounts of degradation

336  intermediates varied remarkably (Figure 5). Comparing to direct photolysis, the pure $TiO_2$

337  catalyst showed 27 times, 12 times, and 76 times increase in hydroxyibuprofen,

338  carboxyibuprofen, and oxypropyl ibuprofen, respectively, owing to the degradation of parent

339  compound (ibuprofen). When the BN content increased to 3% (TB1), the amount of degradation

340  intermediates showed 4%, 60%, and 28% reduction relative to the pure $TiO_2$. The catalysts with

341  5% BN (TB2) also showed a similar increase in degradation intermediates. However, when the

342  BN content increased to 7% (TB3) and 10% (TB4), the degradation intermediates decreased by

343  over 99%, 99%, and 90% for hydroxyibuprofen, carboxyibuprofen, and oxypropyl ibuprofen,

344  respectively, comparing to the pure $TiO_2$. Hence, the increasing BN content of the catalyst

345  facilitated the breakdown of ibuprofen degradation intermediates. However, the further

346  degradation products were not detected with (+) ESI LC-MS/MS probably due to the low

347  concentration of these compounds. These degradation products with smaller carbon chains might

348  be adsorbed onto the catalysts surface and degraded much faster than ibuprofen and its initial

349  degradation intermediates. More analysis of degradation mechanism was discussed in the

350  following Section 3.5.
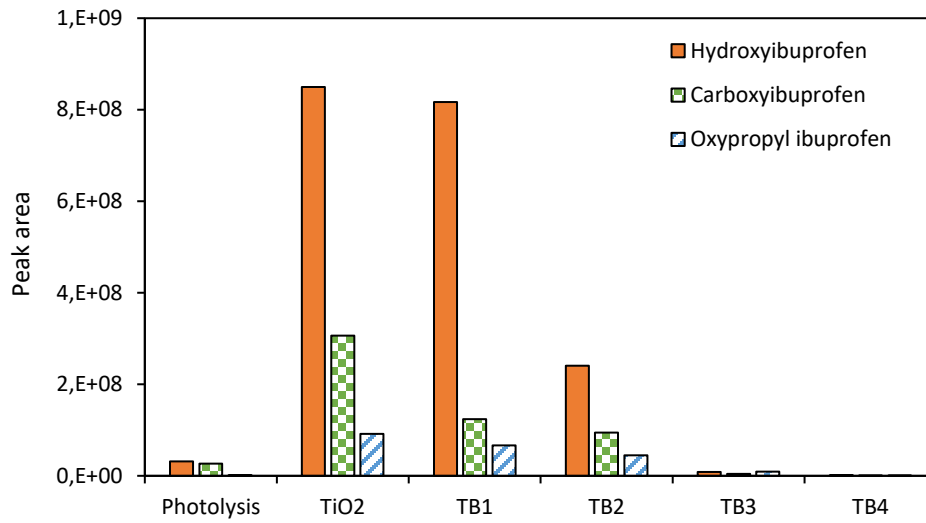
351

Figure 5. Extracted-ion chromatographic peak areas for the precursor masses of ibuprofen

degradation intermediates derived from (+) ESI LC-MS/MS chromatograms from different

catalyst conditions.
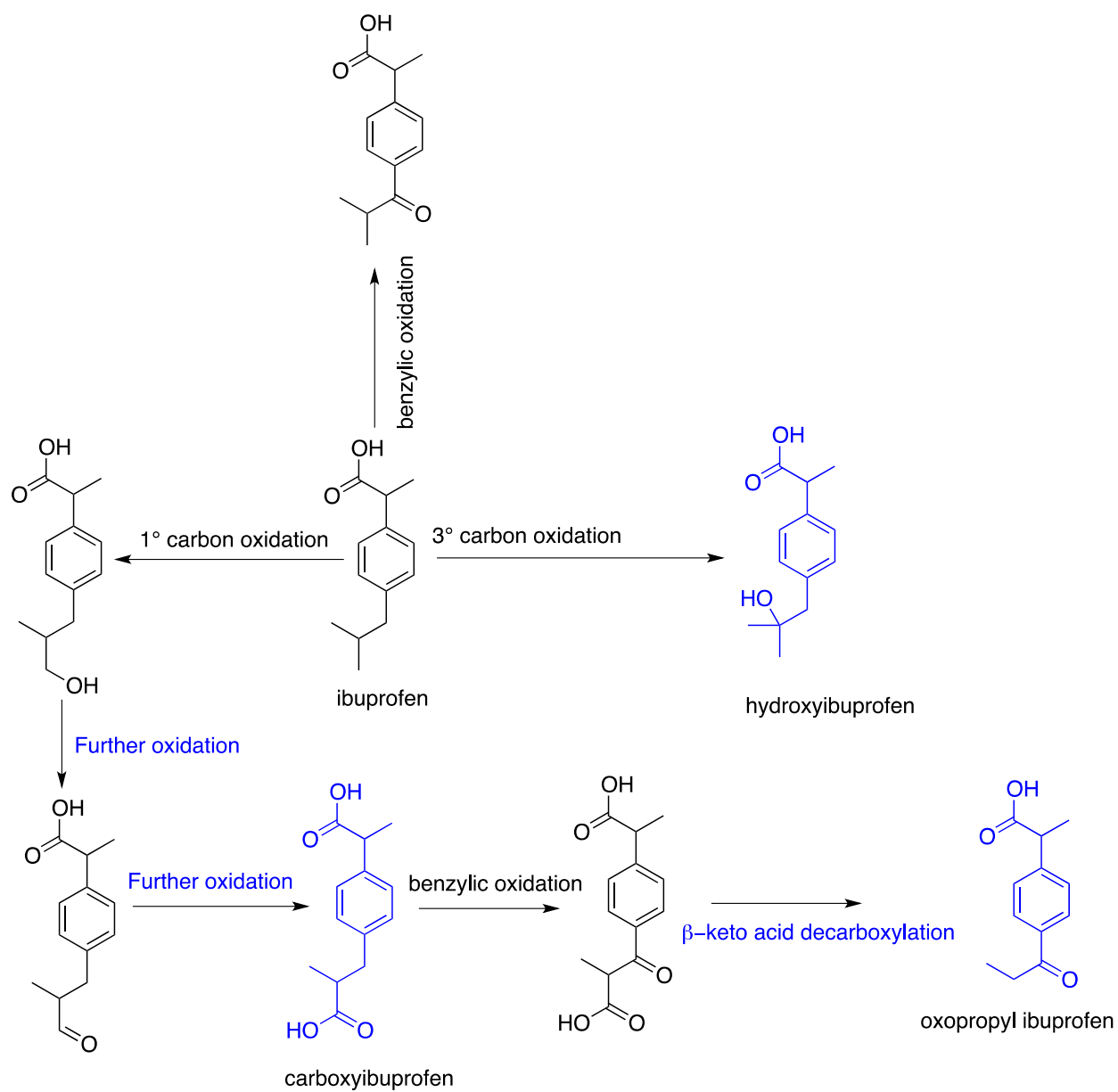
Figure 6. Proposed degradation of ibuprofen by TiO$_2$-BN photocatalysis. Indicated structures were confirmed by mass spectrometry as described.

355

356

357

358

359    3.5    Photocatalytic oxidation mechanisms of ibuprofen

360    The nanocomposite TB4 was chosen to investigate the photocatalytic degradation mechanism of

361    ibuprofen because of its highest photocatalytic activity among the $TiO_2$-BN nanocomposites. The

362    photodegradation of ibuprofen was analyzed in terms of HPLC, FEEM, DOC, $UV_{254}$, and SUVA

363    measurements (Figure 7). The concentration measured by HPLC was the exact concentration of

364    ibuprofen (parent compound); its concentration reduced rapidly and almost completely

365    disappeared after 2-hour reaction. DOC includes all organic carbons in parent compounds,

366    degradation intermediates and products, serving as an indicator for mineralization degree.

367    Compared with the ibuprofen removal results from the HPLC analysis, the DOC reduction was

368    much slower, with only 25% after 2-h reaction. Although the TB4 was effective to oxidize

369    ibuprofen at a fast rate, the organic intermediates from the ibuprofen oxidation need longer time

370    to be mineralized.
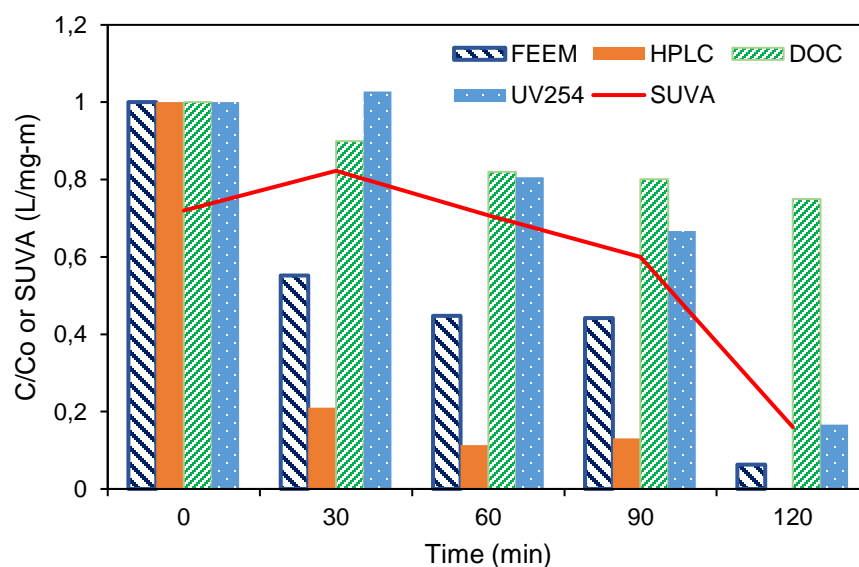
371



372    Figure 7. Reduction of DOC, FEEM peak values, and SUVA values during photocatalytic

373                           oxidation of ibuprofen using TB4 under UV irradiation

375  The UV$_{254}$ and SUVA are used to determine the removal of aromatic fractions of ibuprofen

376  (Stoll et al., 2015). As shown in Figure 7, the SUVA and UV$_{254}$ results exhibited a similar

377  removal trend suggesting aromatic fraction of ibuprofen was degraded. Even though ibuprofen

378  concentration reduced by 79% for the first 30 min, there were 14% and 3% increases in terms of

379  SUVA and UV$_{254}$, respectively. The degradation of ibuprofen was further characterized by the

380  FEEM spectroscopy. The fluorescence peak disappeared after 2-hour of treatment (Figure S3).

381  The excitation-emission peak observed at 220 nm/285 nm corresponds to aromatic compounds

382  (Chen et al., 2003). The fluorescence peak volume was used to compare the aromatic fractions in

383  the tested ibuprofen solution at different reaction time (Figure 7). The peak volume reduced by

384  94% after 2-hour reaction, supporting the decrease in aromatic compounds, consistent with the

385  results of UV$_{254}$ and SUVA that aromatic organic carbon was removed from the solution.

386  The results implied that the intermediates become more aromatic than the parent compound after

387  a partial oxidation. As discussed in Section 3.4, intermediates with more complex structure were

388  detected after photocatalytic treatment. Interestingly, there was only 13% reduction of ibuprofen

389  concentration in the last 30 min of reaction (from 90 to 120 min), but SUVA, UV$_{254}$, and FEEM

390  decreased by 61%, 50%, and 38%, respectively. It suggested that decomposition from parent

391  compounds to intermediates happened mainly during the initial 90 min, while degradation of

392  intermediates into shorter carbon chains occurred mainly after decomposition. Besides, the DOC

393  reduction in the first 30 min probably attributed to the adsorption of ibuprofen onto TB4 (Figure

394  3), the mineralization of ibuprofen was a slow process in the following 90 min due to the tardy

395  reduction of DOC. These results demonstrated that photocatalytic oxidation of ibuprofen

396    molecules by the synthesized nanofibers is a complex multi-step process, degradation of

397    intermediates is probably a control step for the ibuprofen photocatalytic oxidation.

398

399    3.6      Recyclability of the synthesized catalysts

400    The recyclability of the photocatalysts by reusing the catalysts in multiple treatment cycles is

401    crucial in accessing the practical application of a catalyst, because the catalyst may be poisoned

402    by some species (e.g., reaction intermediates) during the reaction process, or may otherwise

403    decompose. In the present work, the recyclability of the pure $TiO_2$ and TB4 was investigated by

404    performing 16 UV irradiation cycles. In each cycle, UV light was irradiated for 3-hour at room

405    temperature. The adsorption of ibuprofen by $TiO_2$ and TB4 achieved 65% and 41% after 3-hour

406    mixing (Figure 2), but the photocatalytic activity of $TiO_2$ and TB4 still remained 80% and 79%

407    after eight cycles of photocatalytic reaction (Figure 8).

408    After eight cycles, the used nanofibers were irradiated by the UV lamp for 3-hour in deionized

409    water. The treatment efficiency was recovered to 98% and 95% for TB4 and $TiO_2$ after 3-hour

410    regeneration by UV irradiation. However, the degradation efficiency of ibuprofen receded

411    gradually in the following eight cycles, although the TB4 remarkably outperformed $TiO_2$.

412    According to Section 3.4, more ibuprofen and intermediates were detected for $TiO_2$ than TB4,

413    hence, weaker photocatalytic activity is probably attributed to the generation and accumulation

414    of intermediates during the catalytic process, which remained on the catalyst and may restrain

415    the further adsorption and degradation of ibuprofen. In addition to the UV irradiation as an

416    effective method for the regeneration of exhausted nanofibers, chemical regeneration should also

417    be studied to fully restore the photocatalysts.
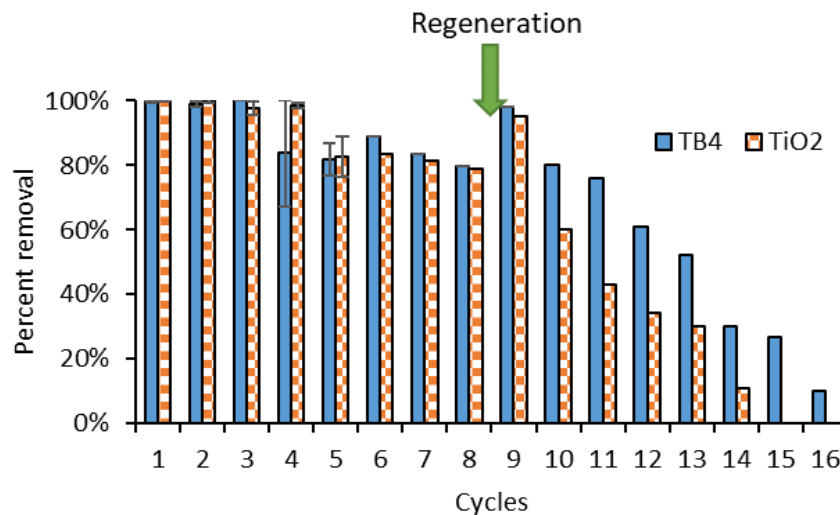
Figure 8. Ibuprofen removal efficiency of TB4 and $TiO_2$ catalysts during multiple photocatalytic cycles under the irradiation of UV light

## 4. Conclusions

The adsorption, photolysis, and photocatalytic oxidation of ibuprofen by $TiO_2$-BN nanocomposites were studied using a multiple analysis approach. The degradation kinetics, mechanisms, and intermediate products were elucidated. The primary conclusions of the study are summarized as follows.

- Wrapping BN nanosheets onto $TiO_2$ nanofibers improved light absorption efficiency and specific surface area of $TiO_2$ nanofibers, and enhanced separation effectiveness of photogenerated $e^-$-$h^+$ pairs.

- Both adsorption and photocatalytic oxidation of ibuprofen by the $TiO_2$-BN nanocomposites followed the first-order kinetic models. The amount of adsorbed ibuprofen at

432  equilibrium reached approximately 14 mg $g^{-1}$ for the $TiO_2$-BN photocatalysts. The

433  photocatalytic degradation rate increased with the increasing BN content.

434  • Analysis of degradation intermediates suggested that the increasing BN content of the

435  catalyst facilitated the breakdown of ibuprofen degradation intermediates (hydroxyibuprofen,

436  carboxyibuprofen, and oxypropyl ibuprofen). No further degradation intermediates were detected

437  by the (+) ESI LC-MS/MS chromatograms likely due to lower concentrations of these

438  compounds.

439  • Multiple photocatalytic cycles were conducted to investigate the reusability of the

440  photocatalysts. UV irradiation of the catalysts in clean water could recover the degradation

441  efficiency to 98% and 95% for TB4 and $TiO_2$. However, photocatalytic activity receded

442  gradually, especially $TiO_2$, as a result of the accumulation of intermediates during the catalytic

443  process. Further chemical regeneration should be investigated to fully recover the photocatalysts.

444  • Combining $TiO_2$ nanofibers with BN nanosheets provides an innovative method to

445  improve the photocatalytic performance for the degradation of organic contaminants. Further

446  studies on photocatalytic oxidation of organic contaminants of emerging concerns should be

447  conducted using solar light in environmental conditions (e.g., wastewater).

448

453

455 **References**

456  Andreozzi, R., Caprio, V., Insola, A., Marotta, R., 1999. Advanced oxidation processes (AOP) for water
457  purification and recovery. Catalysis Today 53, 51-59.
458 Arlos, M.J., Liang, R., Hatat-Fraile, M.M., Bragg, L.M., Zhou, N.Y., Servos, M.R., Andrews, S.A., 2016.
459 Photocatalytic decomposition of selected estrogens and their estrogenic activity by UV-LED irradiated
460 TiO2 immobilized on porous titanium sheets via thermal-chemical oxidation. J Hazard Mater 318, 541-
461 550.
462 Asiltürk, M., Sayılkan, F., Arpaç, E., 2009. Effect of Fe3+ ion doping to TiO2 on the photocatalytic
463 degradation of Malachite Green dye under UV and vis-irradiation. Journal of Photochemistry and
464 Photobiology A: Chemistry 203, 64-71.
465 Bauer, C., Jacques, P., Kalt, A., 2001. Photooxidation of an azo dye induced by visible light incident on
466 the surface of TiO 2. Journal of Photochemistry and Photobiology A: Chemistry 140, 87-92.
467 Biscarat, J., Bechelany, M., Pochat-Bohatier, C., Miele, P., 2015. Graphene-like BN/gelatin
468 nanobiocomposites for gas barrier applications. Nanoscale 7, 613-618.
469 Blake, D., 2001. Bibliography of Work on the Heterogeneous Photocatalytic Removal of Hazardous
470 Compounds from Water and Air--Update Number 4 to October 2001. National Renewable Energy Lab.,
471 Golden, CO (US).
472 Carbonaro, S., Sugihara, M.N., Strathmann, T.J., 2013. Continuous-flow photocatalytic treatment of
473 pharmaceutical micropollutants: Activity, inhibition, and deactivation of TiO2 photocatalysts in
474 wastewater effluent. Applied Catalysis B: Environmental 129, 1-12.
475 Chen, W., Westerhoff, P., Leenheer, J.A., Booksh, K., 2003. Fluorescence Excitation−Emission Matrix
476 Regional Integration to Quantify Spectra for Dissolved Organic Matter. Environmental Science &
477 Technology 37, 5701-5710.
478 Christen, V., Hickmann, S., Rechenberg, B., Fent, K., 2010. Highly active human pharmaceuticals in
479 aquatic systems: A concept for their identification based on their mode of action. Aquatic Toxicology 96,
480 167-181.
481 Coleman, H.M., Eggins, B.R., Byrne, J.A., Palmer, F.L., King, E., 2000. Photocatalytic degradation of 17-β-
482 oestradiol on immobilised TiO2. Appl. Catal., B 24, L1-L5.
483 Dalrymple, O.K., Yeh, D.H., Trotz, M.A., 2007. Removing pharmaceuticals and endocrine-disrupting
484 compounds from wastewater by photocatalysis. Journal of Chemical Technology & Biotechnology 82,
485 121-134.
486 De la Cruz, N., Giménez, J., Esplugas, S., Grandjean, D., De Alencastro, L., Pulgarin, C., 2012. Degradation
487 of 32 emergent contaminants by UV and neutral photo-fenton in domestic wastewater effluent
488 previously treated by activated sludge. water research 46, 1947-1957.
489 De Witte, B., Dewulf, J., Demeestere, K., Van Langenhove, H., 2009. Ozonation and advanced oxidation
490 by the peroxone process of ciprofloxacin in water. Journal of Hazardous Materials 161, 701-708.
491 Doll, T.E., Frimmel, F.H., 2004. Kinetic study of photocatalytic degradation of carbamazepine, clofibric
492 acid, iomeprol and iopromide assisted by different TiO2 materials—determination of intermediates and
493 reaction pathways. Water Research 38, 955-964.
494 Fujishima, A., Rao, T.N., Tryk, D.A., 2000. Titanium dioxide photocatalysis. Journal of Photochemistry and
495 Photobiology C: Photochemistry Reviews 1, 1-21.
496 Harifi, T., Montazer, M., 2014. Fe3+:Ag/TiO2 nanocomposite: Synthesis, characterization and
497 photocatalytic activity under UV and visible light irradiation. Applied Catalysis A: General 473, 104-115.
498 Homem, V., Santos, L., 2011. Degradation and removal methods of antibiotics from aqueous matrices –
499 A review. Journal of Environmental Management 92, 2304-2347.

500     Houas, A., Lachheb, H., Ksibi, M., Elaloui, E., Guillard, C., Herrmann, J.-M., 2001. Photocatalytic
501     degradation pathway of methylene blue in water. Appl. Catal., B 31, 145-157.
502     Hu, C., Tang, Y., Jimmy, C.Y., Wong, P.K., 2003. Photocatalytic degradation of cationic blue X-GRL
503     adsorbed on TiO 2/SiO 2 photocatalyst. Applied Catalysis B: Environmental 40, 131-140.
504     Huerta-Fontela, M., Galceran, M.T., Ventura, F., 2011. Occurrence and removal of pharmaceuticals and
505     hormones through drinking water treatment. Water Research 45, 1432-1442.
506     Jing, L., Qu, Y., Wang, B., Li, S., Jiang, B., Yang, L., Fu, W., Fu, H., Sun, J., 2006. Review of
507     photoluminescence performance of nano-sized semiconductor materials and its relationships with
508     photocatalytic activity. Solar Energy Materials and Solar Cells 90, 1773-1787.
509     Konstantinou, I.K., Albanis, T.A., 2004. TiO2-assisted photocatalytic degradation of azo dyes in aqueous
510     solution: kinetic and mechanistic investigations. Applied Catalysis B: Environmental 49, 1-14.
511     Kormann, C., Bahnemann, D., Hoffmann, M.R., 1991. Photolysis of chloroform and other organic
512     molecules in aqueous titanium dioxide suspensions. Environmental science & technology 25, 494-500.
513     Kumar, S.G., Devi, L.G., 2011a. Review on modified TiO2 photocatalysis under UV/visible light: selected
514     results and related mechanisms on interfacial charge carrier transfer dynamics. J Phys Chem A 115,
515     13211-13241.
516     Kumar, S.G., Devi, L.G., 2011b. Review on modified TiO2 photocatalysis under UV/visible light: selected
517     results and related mechanisms on interfacial charge carrier transfer dynamics. J. Photochem. Photobiol.,
518     A 115, 13211-13241.
519     Le-Clech, P., Lee, E.-K., Chen, V., 2006. Hybrid photocatalysis/membrane treatment for surface waters
520     containing low concentrations of natural organic matters. Water Research 40, 323-330.
521     Lee, C.-R., Kim, H.-S., Jang, I.-H., Im, J.-H., Park, N.-G., 2011. Pseudo First-Order Adsorption Kinetics of
522     N719 Dye on TiO2 Surface. ACS Applied Materials & Interfaces 3, 1953-1957.
523     Lee, Y., von Gunten, U., 2010. Oxidative transformation of micropollutants during municipal wastewater
524     treatment: Comparison of kinetic aspects of selective (chlorine, chlorine dioxide, ferrateVI, and ozone)
525     and non-selective oxidants (hydroxyl radical). Water Research 44, 555-566.
526     Li, S., Hu, J., 2018. Transformation products formation of ciprofloxacin in UVA/LED and UVA/LED/TiO2
527     systems: Impact of natural organic matter characteristics. Water Res 132, 320-330.
528     Li, Y., Li, X., Li, J., Yin, J., 2006. Photocatalytic degradation of methyl orange by TiO2-coated activated
529     carbon and kinetic study. Water Res. 40, 1119-1126.
530     Lin, L., Jiang, W., Xu, P., 2017a. Comparative study on pharmaceuticals adsorption in reclaimed water
531     desalination concentrate using biochar: Impact of salts and organic matter. Sci Total Environ 601-602,
532     857-864.
533     Lin, L., Wang, H., Jiang, W., Mkaouar, A.R., Xu, P., 2017b. Comparison study on photocatalytic oxidation
534     of pharmaceuticals by TiO2-Fe and TiO2-reduced graphene oxide nanocomposites immobilized on
535     optical fibers. J Hazard Mater 333, 162-168.
536     Lin, L., Wang, H., Jiang, W., Mkaouar, A.R., Xu, P., 2017c. Comparison study on photocatalytic oxidation
537     of pharmaceuticals by TiO 2-Fe and TiO 2-reduced graphene oxide nanocomposites immobilized on
538     optical fibers. Journal of Hazardous Materials 333, 162-168.
539     Lin, L., Wang, H., Luo, H., Xu, P., 2015. Enhanced photocatalysis using side-glowing optical fibers coated
540     with Fe-doped TiO2 nanocomposite thin films. Journal of Photochemistry and Photobiology A: Chemistry
541     307-308, 88-98.
542     Lin, L., Wang, H., Luo, H., Xu, P., 2016. Photocatalytic Treatment of Desalination Concentrate Using
543     Optical Fibers Coated With Nanostructured Thin Films: Impact of Water Chemistry and Seasonal Climate
544     Variations. Photochem Photobiol 92, 379-387.
545     Lin, L., Wang, H., Xu, P., 2017d. Immobilized TiO2-reduced graphene oxide nanocomposites on optical
546     fibers as high performance photocatalysts for degradation of pharmaceuticals. Chemical Engineering
547     Journal 310, Part 2, 389-398.

548    Lin, L., Wang, H., Xu, P., 2017e. Immobilized TiO 2-reduced graphene oxide nanocomposites on optical
549    fibers as high performance photocatalysts for degradation of pharmaceuticals. Chemical Engineering
550    Journal 310, 389-398.
551    Lin, L., Wang, H., Xu, P., 2017f. Immobilized TiO 2 -reduced graphene oxide nanocomposites on optical
552    fibers as high performance photocatalysts for degradation of pharmaceuticals. Chemical Engineering
553    Journal 310, 389-398.
554    Lin, L., Xu, X., Papelis, C., Xu, P., 2017g. Innovative use of drinking water treatment solids for heavy
555    metals removal from desalination concentrate: Synergistic effect of salts and natural organic matter.
556    Chemical Engineering Research and Design 120, 231-239.
557    Lin, Y., Williams, T.V., Connell, J.W., 2010. Soluble, Exfoliated Hexagonal Boron Nitride Nanosheets. The
558    Journal of Physical Chemistry Letters 1, 277-283.
559    Liqiang, J., Yichun, Q., Baiqi, W., Shudan, L., Baojiang, J., Libin, Y., Wei, F., Honggang, F., Jiazhong, S.,
560    2006. Review of photoluminescence performance of nano-sized semiconductor materials and its
561    relationships with photocatalytic activity. Solar Energy Materials and Solar Cells 90, 1773-1787.
562    Liu, D., Zhang, M., Xie, W., Sun, L., Chen, Y., Lei, W., 2017. Porous BN/TiO2 hybrid nanosheets as highly
563    efficient visible-light-driven photocatalysts. Applied Catalysis B: Environmental 207, 72-78.
564    Lu Lin, X.X., Charalambos Papelis, Tzahi Y. Cath, Pei Xu, 2014. Sorption of metals and metalloids from
565    reverse osmosis concentrate on drinking water treatment solids. Separation and Purification Technology
566    134, 37-45.
567    Lv, Y., Cao, X., Jiang, H., Song, W., Chen, C., Zhao, J., 2016. Rapid photocatalytic debromination on TiO2
568    with in-situ formed copper co-catalyst: Enhanced adsorption and visible light activity. Applied Catalysis B:
569    Environmental 194, 150-156.
570    Merenda, A., Kong, L., Zhu, B., Duke, M.C., Gray, S.R., Dumée, L.F., 2019. Functional Nanoporous
571    Titanium Dioxide for Separation Applications: Synthesis Routes and Properties to Performance Analysis.
572    in: Pannirselvam, M., Shu, L., Griffin, G., Philip, L., Natarajan, A., Hussain, S. (Eds.). Water Scarcity and
573    Ways to Reduce the Impact: Management Strategies and Technologies for Zero Liquid Discharge and
574    Future Smart Cities. Springer International Publishing, Cham, pp. 151-186.
575    Nakajima, T., Xu, Y.-H., Mori, Y., Kishita, M., Takanashi, H., Maeda, S., Ohki, A., 2005. Combined use of
576    photocatalyst and adsorbent for the removal of inorganic arsenic (III) and organoarsenic compounds
577    from aqueous media. Journal of hazardous materials 120, 75-80.
578    Nakata, K., Fujishima, A., 2012. TiO2 photocatalysis: Design and applications. Journal of Photochemistry
579    and Photobiology C: Photochemistry Reviews 13, 169-189.
580    Nalbandian, M.J., Zhang, M., Sanchez, J., Kim, S., Choa, Y.-H., Cwiertny, D.M., Myung, N.V., 2015.
581    Synthesis and optimization of Ag–TiO 2 composite nanofibers for photocatalytic treatment of impaired
582    water sources. Journal of hazardous materials 299, 141-148.
583    Nasr, M., Viter, R., Eid, C., Habchi, R., Miele, P., Bechelany, M., 2017a. Enhanced photocatalytic
584    performance of novel electrospun BN/TiO2composite nanofibers. New J. Chem. 41, 81-89.
585    Nasr, M., Viter, R., Eid, C., Habchi, R., Miele, P., Bechelany, M., 2017b. Enhanced photocatalytic
586    performance of novel electrospun BN/TiO 2 composite nanofibers. New Journal of Chemistry 41, 81-89.
587    Ollis, D.F., Hsiao, C.-Y., Budiman, L., Lee, C.-L., 1984. Heterogeneous photoassisted catalysis: conversions
588    of perchloroethylene, dichloroethane, chloroacetic acids, and chlorobenzenes. Journal of catalysis 88,
589    89-96.
590    Ollis, D.F., Pelizzetti, E., Serpone, N., 1991. Photocatalyzed destruction of water contaminants. Environ.
591    Sci. Technol. 25, 1522-1529.
592    Prieto-Rodriguez, L., Miralles-Cuevas, S., Oller, I., Agüera, A., Puma, G.L., Malato, S., 2012. Treatment of
593    emerging contaminants in wastewater treatment plants (WWTP) effluents by solar photocatalysis using
594    low TiO2 concentrations. Journal of Hazardous Materials 211, 131-137.

595    Rioja, N., Benguria, P., Peñas, F., Zorita, S., 2014. Competitive removal of pharmaceuticals from
596    environmental waters by adsorption and photocatalytic degradation. Environmental Science and
597    Pollution Research 21, 11168-11177.

598    Rosenfeldt, E.J., Linden, K.G., 2004. Degradation of Endocrine Disrupting Chemicals Bisphenol A, Ethinyl
599    Estradiol, and Estradiol during UV Photolysis and Advanced Oxidation Processes. Environmental Science
600    & Technology 38, 5476-5483.

601    Rubio, D., Casanueva, J.F., Nebot, E., 2013. Improving UV seawater disinfection with immobilized TiO2:
602    Study of the viability of photocatalysis (UV254/TiO2) as seawater disinfection technology. Journal of
603    Photochemistry and Photobiology A: Chemistry 271, 16-23.

604    Skoumal, M., Rodríguez, R.M., Cabot, P.L., Centellas, F., Garrido, J.A., Arias, C., Brillas, E., 2009. Electro-
605    Fenton, UVA photoelectro-Fenton and solar photoelectro-Fenton degradation of the drug ibuprofen in
606    acid aqueous medium using platinum and boron-doped diamond anodes. Electrochimica Acta 54, 2077-
607    2085.

608    Stoll, Z.A., Forrestal, C., Ren, Z.J., Xu, P., 2015. Shale gas produced water treatment using innovative
609    microbial capacitive desalination cell. J Hazard Mater 283, 847-855.

610    Tanaka, K., Padermpole, K., Hisanaga, T., 2000. Photocatalytic degradation of commercial azo dyes.
611    Water Res. 34, 327-333.

612    Tawkaew, S., Supothina, S., 2008. Preparation of agglomerated particles of TiO2 and silica-coated
613    magnetic particle. Materials Chemistry and Physics 108, 147-153.

614    Thagard, S.M., Stratton, G.R., Dai, F., Bellona, C.L., Holsen, T.M., Bohl, D.G., Paek, E., Dickenson, E.R.,
615    2016. Plasma-based water treatment: development of a general mechanistic model to estimate the
616    treatability of different types of contaminants. Journal of Physics D: Applied Physics 50, 014003.

617    Turchi, C.S., Ollis, D.F., 1990. Photocatalytic degradation of organic water contaminants: Mechanisms
618    involving hydroxyl radical attack. J. Catal. 122, 178-192.

619    Van Doorslaer, X., Dewulf, J., De Maerschalk, J., Van Langenhove, H., Demeestere, K., 2015.
620    Heterogeneous photocatalysis of moxifloxacin in hospital effluent: Effect of selected matrix constituents.
621    Chemical Engineering Journal 261, 9-16.

622    Vautier, M., Guillard, C., Herrmann, J.-M., 2001. Photocatalytic degradation of dyes in water: case study
623    of indigo and of indigo carmine. Journal of Catalysis 201, 46-59.

624    Vieno, N.M., Härkki, H., Tuhkanen, T., Kronberg, L., 2007. Occurrence of Pharmaceuticals in River Water
625    and Their Elimination in a Pilot-Scale Drinking Water Treatment Plant. Environmental Science &
626    Technology 41, 5077-5084.

627    Wang, H., Heil, D., Ren, Z.J., Xu, P., 2015. Removal and fate of trace organic compounds in microbial fuel
628    cells. Chemosphere 125, 94-101.

629    Westerhoff, P., Yoon, Y., Snyder, S., Wert, E., 2005. Fate of endocrine-disruptor, pharmaceutical, and
630    personal care product chemicals during simulated drinking water treatment processes. Environmental
631    science & technology 39, 6649-6663.

632    Wold, A., 1993. Photocatalytic properties of titanium dioxide (TiO2). Chemistry of Materials 5, 280-283.

633    Xiang, Y., Fang, J., Shang, C., 2016. Kinetics and pathways of ibuprofen degradation by the UV/chlorine
634    advanced oxidation process. Water Res 90, 301-308.

635    Xuesong Xu, L.L., Charalambos Papelis, Maung Myint, Tzahi Y. Cath, Pei Xu, 2015. Use of drinking water
636    treatment solids for arsenate removal from desalination concentrate. Journal of Colloid and Interface
637    Science 455, 252-261.

638    Yean, S., Cong, L., Yavuz, C., Mayo, J., Yu, W., Kan, A., Colvin, V., Tomson, M., 2005. Effect of magnetite
639    particle size on adsorption and desorption of arsenite and arsenate. Journal of Materials Research 20,
640    3255-3264.

641    Yi, Z., Merenda, A., Kong, L., Radenovic, A., Majumder, M., Dumée, L.F., 2018. Single step synthesis of
642    Schottky-like hybrid graphene - titania interfaces for efficient photocatalysis. Scientific Reports 8, 8154.

643    Yu, Y., Yu, J.C., Chan, C.-Y., Che, Y.-K., Zhao, J.-C., Ding, L., Ge, W.-K., Wong, P.-K., 2005. Enhancement of
644    adsorption and photocatalytic activity of $TiO_2$ by using carbon nanotubes for the treatment of azo dye.
645    Applied Catalysis B: Environmental 61, 1-11.
646    Zhang, S., Chen, L., Liu, H., Guo, W., Yang, Y., Guo, Y., Huo, M., 2012. Design of $H_3PW_{12}O_{40}/TiO_2$ and
647    $Ag/H_3PW_{12}O_{40}/TiO_2$ film-coated optical fiber photoreactor for the degradation of aqueous rhodamine
648    B and 4-nitrophenol under simulated sunlight irradiation. Chemical Engineering Journal 200-202, 300-
649    309.
650    Zhang, Z., Xiao, F., Guo, Y., Wang, S., Liu, Y., 2013. One-pot self-assembled three-dimensional $TiO_2$-
651    graphene hydrogel with improved adsorption capacities and photocatalytic and electrochemical
652    activities. ACS Appl Mater Interfaces 5, 2227-2233.

653

654

## List of the Figure Captions

Figure 1. XRD patterns of synthesized catalysts. A: anatase; R: rutile.

Figure 2. Adsorption kinetics of ibuprofen onto different photocatalysts. Error bars represent the standard deviation of duplicate experiments.

Figure 3. Photocatalytic kinetics of ibuprofen onto different photocatalysts under UV light irradiation. Error bars represent the standard deviation of duplicate experiments.

Figure 4. Langmuir-Hinshelwood kinetic modeling curves of ibuprofen degradation by the synthesized nanocomposites

Figure 5. Extracted-ion chromatographic peak areas for the precursor masses of ibuprofen degradation intermediates derived from (+) ESI LC-MS/MS chromatograms from different catalyst conditions.

Figure 6. Proposed degradation of ibuprofen by $TiO_2$-BN photocatalysis. Indicated structures were confirmed by mass spectrometry as described.

Figure 7. Reduction of DOC, FEEM peak values, and SUVA values during photocatalytic oxidation of ibuprofen using TB4 under UV irradiation

Figure 8. Ibuprofen removal efficiency of TB4 and $TiO_2$ catalysts during multiple photocatalytic cycles under the irradiation of UV light